Phys. Status Solidi B **252,** No. 10, 2222–2229 (2015) / **DOI** 10.1002/pssb.201552155

physica status solidi b
www.pss-b.com
basic solid state physics

Control of fluorescence enhancement and directionality upon excitations in a thin-film system

Xingxing Chen[1], Yu-Hui Chen[2], Min Qiu[*,1,3], Richard J. Blaikie[,2], and Boyang Ding[***,2]**

[1] Department of Optical Engineering, State Key Laboratory of Modern Optical Instrumentation, Zhejiang University, Hangzhou 310027, P.R. China
[2] Department of Physics, MacDiarmid Institute, for Advanced Materials and Nanotechnology, University of Otago, Dunedin 9016, New Zealand
[3] School of Information and Communication Technology, Royal Institute of Technology, Electrum 229, Kista 16440, Sweden

Received 23 March 2015, revised 3 April 2015, accepted 8 May 2015
Published online 7 July 2015

Keywords dynamic manipulation, Fabry–Perot resonances, fluorescence, surface plasmon polaritons, thin films

[*] Corresponding author: e-mail minqiu@zju.edu.cn, Phone/Fax: +86 571 87953159
[**] e-mail richard.blaikie@otago.ac.nz, Phone: +64 3 479 8835, Fax: +64 3 479 0964
[***] e-mail boyang.ding@otago.ac.nz, Phone: +64 3 479 7784, Fax: +64 3 479 0964

Nanostructures with various configurations have been extensively used to engineer the emission properties of embedded fluorophores, but lack the flexibility to dynamically control fluorescence. Here we report a thin-film cavity system, comprising a quarter wavelength thick dye-doped dielectric coating on a reflecting surface, in which the fluorescence enhancement and directionality can be significantly modified by altering the illumination angle. The configuration of the cavity yields absorption properties that are highly dependent on illumination angles, due to the coupling between molecular absorption and Fabry–Perot resonances. Therefore the fluorescence intensity relating to the angle-dependent absorbing efficiency varies with illumination angles. In addition, as a result of synergy between intrinsic absorption of the reflecting surface, Fabry–Perot and surface-plasmon-polariton resonances and illumination-angle dependent excitation efficiencies for differently located molecules, the global emission intensity, including emission from dyes at all locations, can be directionally redistributed by altering the illumination angle.

1 Introduction Fluorescence is a process of photon emission from excited fluorophores. The emission properties of a fluorophore, e.g., fluorescence intensity, lifetime, and emission directionality, can be engineered through coupling with the electromagnetic (EM) resonances in various photonic nanostructures, such as metallic nanoparticles [1–10], optical antennas [11–15], and photonic/plasmonic crystals [16–19]. This is because photonic nanostructures can create a structure-defined complex dielectric environment that interacts with EM waves. As the result, previous studies mainly focus on integrating fluorophores into nanostructures with various configurations to manipulate their emission properties, which, however, fails to dynamically control the fluorescence emission, because it is difficult to modify the configuration of a ready-made nanostructure.

On the other hand, dynamic control of fluorescence properties is highly desirable for real life applications. In this context, several novel measures have been used to flexibly tune the emission of fluorophores embedded in photonic nanostructures. For example, Almpanis et al. demonstrated the modulation of spontaneous emission from a stratified nanostructure based on acousto-optic interaction [20]. Stress-responsive photonic crystals [21, 22] have also been used to adjust the emission behaviors. In this report, we propose that if a photonic nanostructure can be properly designed that its absorbing behaviors are sensitive to the change of illumination conditions, e.g., the angle, polarization, and wavelength of illumination, one may be able to dynamically tune the emission properties of fluorophores embedded in this photonic nanostructure by adjusting the illumination/excitation conditions. Previous studies generally neglect the influence of the excitation conditions, because it is commonly assumed that the absorbing properties of the nanostructures are identical for

different illuminations and fluorophores located at different positions within the nanostructures are equally excited during the excitation process. This, nevertheless, is not completely true in reality, since the complex dielectric environment created by nanostructures not only interacts with the emitted photons but also influences the excitation fields. As a result, the absorption properties of nanostructures may fluctuate for different illumination conditions. In addition, the field distribution of the excitation wave within nanostructures may also be modified by applying different illumination conditions, thus unequally exciting fluorophores at different locations. These factors may give rise to significant modification of emission properties, hence altering the excitation conditions in concert with the structure-defined EM environment can be used to manipulate fluorescence properties.

Specifically, in this report, we experimentally and numerically prove that in a fluorophore-embedded nanoscale thin-film cavity, altering the illumination angle (θ_{exc}) of the excitation laser allows us to flexibly modify the fluorescence enhancement with respect to a reference sample and directionally redistribute the emission intensity. The thin-film cavity presented here comprises of a 95 ± 3 nm thick Polyvinyl Alcohol (PVA) film doped with Rhodamine 6G (R6G) molecules on an optically thick silver (Ag) substrate (left-hand schematic in Fig. 1). The reference samples were prepared by coating the same R6G doped PVA (PVA_{R6G}) film on a glass substrate. Earlier reports [23–25] showed that, in such a thin-film cavity, the emission can be enhanced through coupling with Surface Plasmon Polaritons (SPPs) propagating along the interface between the dielectric coating and the reflecting surface. In our experiment, it turns out that the fluorescence intensity from the thin-film cavity varies with different illumination angles. This is because the thickness of the PVA_{R6G} coating was carefully chosen to be, where λ is the wavelength and n is the refractive index of the PVA_{R6G}, satisfying the excitation conditions of Fabry–Perot (FP) resonances at oblique incidence in the Ag substrate sample [26]. As a result, the absorbing efficiency of the PVA_{R6G} coatings on Ag substrates (PVA_{R6G}–Ag) is very sensitive to the angle of incidence, due to the coupling between FP resonances and molecular absorption [26], thus leading to the variation of fluorescence intensity with illumination angles, which can be revealed by comparing angle-resolved absorption and fluorescence spectra.

Previous studies also demonstrate that in the thin-film cavity if the reflecting layer is semi-transparent and combined with a glass prism (or a glass substrate), the excited fluorophores near the reflecting surface can radiate into the underlying glass prism, through coupling with SPPs excited at the interface between the reflecting layer and the prism [27–30], known as Surface Plasmon Coupled Emission (SPCE). In addition, the coupling strength between the excited fluorophores and SPPs is highly dependent on the distance between fluorophores and the reflecting surface, hereafter referred to the fluorophore-interface or dipole-interface distance [27, 31]. Furthermore, together with the intrinsic absorption of the reflecting surface [27, 31, 32], the interference [33–36] between the fluorescence radiation and the reflected waves from the reflecting surface can also alter the decaying properties of the excited fluorophores, which are highly dependent on the fluorophore-interface distance too [31]. Therefore, if a dielectric spacer layer is introduced as a separation between the dye layer and the reflecting surface, by adjusting the thickness of the dielectric spacer, the resulting multilayer system can be used to manipulate the fluorescence lifetime [31–33, 37–43] and the emission directionality [33–36], because the inclusion of the spacer layer allows us to precisely control the fluorophore-interface distance. Yet, similar to previous studies in other kinds of nanostructures, most of the investigations in the fluorophore-embedded thin-film cavity are still based on using different physical configurations to engineer the fluorescence properties. In contrast, the directionality of the fluorescence from our PVA_{R6G}–Ag sample can be tuned by altering the illumination angles. Our simulation shows that this is because the excitation efficiency for a molecule at a specific location within the thin-film structure closely relates to the intensity distribution of the excitation wave, which changes with different excitation angles. In addition, the radiation directionality of a single molecule varies with its location. As a result, the angular distribution of the overall radiation, which is integrated from molecules at all locations, can be modified by altering the excitation angles, giving rise to the illumination angle dependent fluorescence directionality.

2 Experimental details In our experiment, aqueous PVA solution doped with R6G molecules of a low concentration (0.5 mM) was spin-coated on an optically thick Ag substrate, which was prepared by thermally evaporating 130 nm Ag on a polished silicon substrate. The thickness of the PVA_{R6G} coating is controlled at 95 ± 3 nm, achieved by adjusting the spinning speed and the density of PVA in the solution. The same PVA_{R6G} coating was spun on a glass substrate as a reference sample.

The angle-resolved fluorescence measurement (upper-right schematic in Fig. 1) was performed using a customised set-up as previously reported [17]. Specifically, the fluorescence spectra were collected by a spectrometer in a wide range of fluorescence angle $\Delta\theta_{FL}$ ($0^o - 80^o$) with a resolution of 5^o from samples illuminated by a continuous-wave (CW) green laser ($\lambda_{exc} = 532$ nm) with various excitation angle ($\theta_{exc} = 5^o, 30^o, 60^o$). The fluorescence spectra were acquired with s- and p- polarizations, defined as the electric field being perpendicular or parallel to the plane of illumination, by placing an analyzer before the spectrometer. A polarizer is used to set the polarization of the illumination beam before it excites the sample. The angle-resolved absorption spectra were calculated by subtracting the white light incidence with the reflection (for both PVA_{R6G}–Ag and PVA_{R6G}–glass samples) and

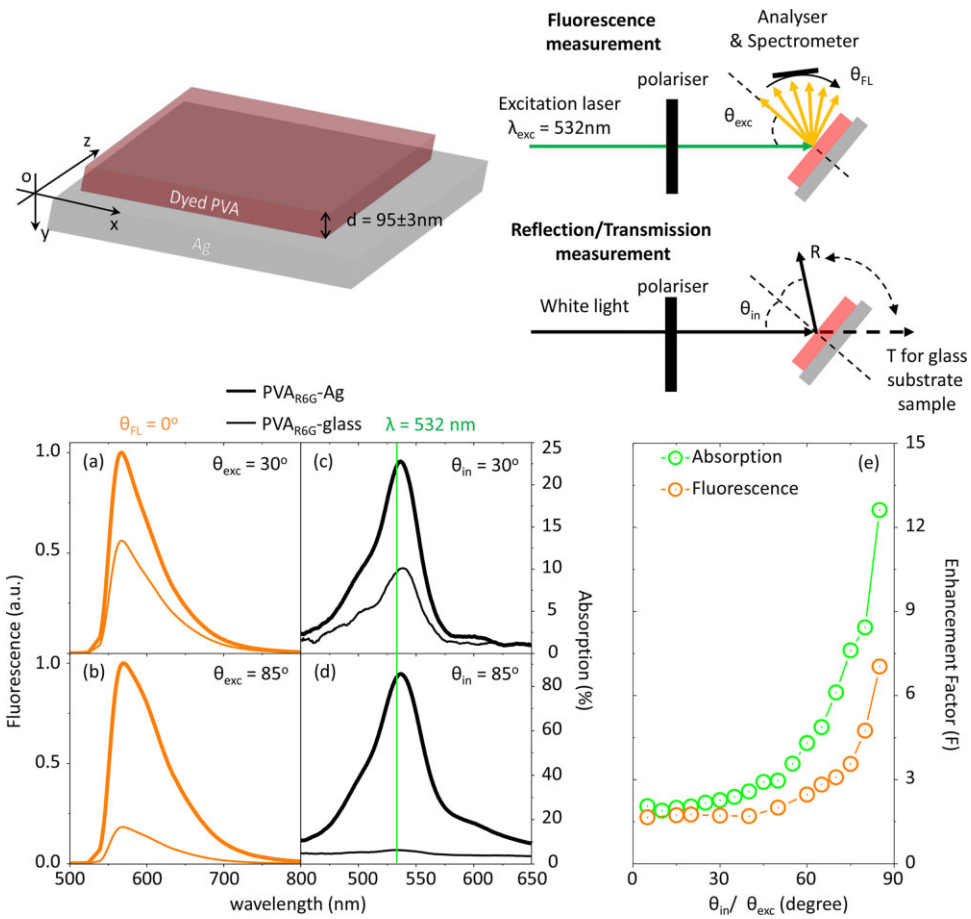

Figure 1 Dye-doped nanoscale thin-film system and its fluorescence and absorption spectra. Top-left schematic: the PVA_{R6G}–Ag thin film structure; right-hand schematic: the experimental setup for the angle-resolved fluorescence measurement (upper-right) and the angle-resolved transmission/reflection measurement (lower-right). Bottom: (a,b) Fluorescence emission spectra collected at $\theta_{FL} = 0^o$ of the PVA_{R6G}–Ag (orange thick line) and PVA_{R6G}–glass (orange thin line) excited by s-polarized laser ($\lambda_{exc} = 532\,nm$) with the excitation angle $\theta_{exc} = 30^o$ (a) and $\theta_{exc} = 85^o$ (b). (c,d) Absorption spectra measured for the PVA_{R6G}–Ag (black thick line) and PVA_{R6G}–glass (black thin line) under s-polarized illumination with incident angle (c) $\theta_{in} = 30^o$ and (d) $\theta_{in} = 85^o$. (e) Enhancement factor of the absorption (green dotted circle) at $\lambda = 532\,nm$ and the fluorescence (orange dotted circle) integrated over the spectral range $\Delta\lambda_{FL}$ (550–800 nm). Green solid line in (c) and (d) indicates the spectral position of the excitation laser.

transmission (for PVA_{R6G}–glass only) measured using a setup as illustrated in lower-right schematic of Fig. 1 at each incident angle θ_{in} with a specific polarization.

3 Experimental results and discussion Turning to the details of experiment results, Fig. 1a shows the fluorescence spectra measured at the normal emission angle ($\theta_{FL} = 0^o$) for samples of PVA_{R6G}–Ag and PVA_{R6G}–glass (reference sample), under the same excitation conditions ($\lambda_{exc} = 532\,nm$, s-polarized and $\theta_{exc} = 30^o$). As can be seen, the magnitude of the fluorescence at its maximum ($\lambda = 560\,nm$) for the PVA_{R6G}–Ag sample is approximately two times as for the reference sample. For higher excitation angle ($\theta_{exc} = 85^o$), the fluorescence enhancement at the maximum is increased up to approximately sevenfold, as shown in Fig. 1b. The absorption spectra of the PVA_{R6G}–Ag and PVA_{R6G}–glass sample acquired at the corresponding incident angles $\theta_{in} = 30^o$ and $\theta_{in} = 85^o$ are shown in Fig. 1c and d, respectively. At the spectral position of the excitation laser ($\lambda = 532\,nm$, indicated by the green solid line in Fig. 1c and d), under s-polarized illumination at, the absorption for the PVA_{R6G}–Ag sample is enhanced as compared to the reference sample up to ~2.2-fold (from 9.7% to 22%); while at $\theta_{in} = 85^o$ the absorption enhancement increases up to ~13-fold (from 6.7% to 86%). In other words, both the absorption and fluorescence enhancement show an illumination angle dependence, the full picture of which can be revealed by calculating the absorption and fluorescence enhancement factors,

$$F_{Absorp}(\theta_{in}) = \frac{\int_{\lambda_{exc}} A_{Ag}(\lambda,\theta_{in})d\lambda}{\int_{\lambda_{exc}} A_{glass}(\lambda,\theta_{in})d\lambda};$$
$$F_{FL}(\theta_{exc}) = \frac{\int_{\Delta\lambda_{FL}} I_{Ag}(\lambda,\theta_{exc})d\lambda}{\int_{\Delta\lambda_{FL}} I_{glass}(\lambda,\theta_{exc})d\lambda}. \quad (1)$$

The absorption enhancement factor F_{Absorp} as a function of the incident angle θ_{in} is defined by normalizing the absorption of a $\mathrm{PVA_{R6G}}$–Ag sample, denoted as, to the absorption of the reference sample, denoted as, at the excitation wavelength ($\lambda = 532$ nm); while the fluorescence enhancement factor F_{FL} as a function of the excitation angle, was calculated by comparing the fluorescence collected at $\theta_{\mathrm{FL}} = 0^{\mathrm{o}}$ for a $\mathrm{PVA_{R6G}}$–Ag sample ($I_{\mathrm{Ag}}(\lambda, \theta_{\mathrm{exc}})$) with that for the reference sample ($I_{\mathrm{glass}}(\lambda, \theta_{\mathrm{exc}})$) integrated over the full fluorescence spectral range $\Delta\lambda_{\mathrm{FL}}$ (500–800 nm). As shown in Fig. 1e, it is evident to see that both F_{Absorp} and F_{FL} show a similar exponentially increasing tendency towards more oblique illumination. As we discussed in Ref. [26], the enhanced absorption in the $\mathrm{PVA_{R6G}}$–Ag sample is the result of coupling between the molecular absorption and FP resonances, since the $\mathrm{PVA_{R6G}}$ coating with properly chosen thickness together with the Ag substrate forms a resonant cavity in which FP resonances can be excited and are very sensitive to the angle of incidence. In other words, the $\mathrm{PVA_{R6G}}$–Ag sample behaves like a platform increasing the effective optical absorption cross-section of the embedded fluorophores, thus being able to enhance the emission intensity under the same excitation conditions, which is similar to the result presented in Ref. [37]. However, the magnitudes of F_{FL} are always lower than that of F_{Absorp} at the corresponding incident/excitation angles and the difference between F_{Absorp} and F_{FL} becomes even larger at highly oblique illumination, implying the fluorescence enhancement does not compete with the absorption enhancement. This cannot be addressed by the absorption of Ag substrates to the excitation energy, since our simulation (Fig. S1 in Supporting Information) shows the fraction of the incident energy being absorbed by the $\mathrm{PVA_{R6G}}$ coating becomes higher if the $\mathrm{PVA_{R6G}}$–Ag sample is illuminated at a more oblique angle. Two factors may account for the unmatched enhancement rate between absorption and fluorescence: (i) the presence of Ag substrates may provide additional non-radiative decay channels to the fluorescence [27, 31, 32] and (ii) the angular distribution of the fluorescence intensity for the $\mathrm{PVA_{R6G}}$–Ag sample may be different from that for the reference sample at the same excitation angles, given that the fluorescence enhancement factor shown in Fig. 1e is calculated only for the normal emission ($\theta_{\mathrm{FL}} = 0^{\mathrm{o}}$).

The angular distribution of fluorescence intensity, integrated over the spectral range $\Delta\lambda_{\mathrm{FL}}$ (500–800 nm), for the $\mathrm{PVA_{R6G}}$–glass and $\mathrm{PVA_{R6G}}$–Ag samples excited by the s-polarized laser at the same excitation angles ($\theta_{\mathrm{exc}} = 5^{\mathrm{o}}, 30^{\mathrm{o}}, 60^{\mathrm{o}}$), has been measured and is shown as polar patterns in Fig. 2. While excited with $\theta_{\mathrm{exc}} = 5^{\mathrm{o}}$, the fluorescence intensity for the $\mathrm{PVA_{R6G}}$–glass sample (Fig. 2a) shows its maximum at $\theta_{\mathrm{FL}} = 0^{\circ}$, and then gradually declines as θ_{FL} increases, regardless of the emission polarizations, exhibiting the same directionality as the Lambert's cosine law (black dashed line in Fig. 2a) predicts [17, 41]. Excitation with other angles (Fig. 2b for $\theta_{\mathrm{exc}} = 30^{\mathrm{o}}$ and Fig. 2c for $\theta_{\mathrm{exc}} = 60^{\mathrm{o}}$) gives the same results as in the case of $\theta_{\mathrm{exc}} = 5^{\mathrm{o}}$, manifesting changing the excitation angle applies no influence on the fluorescence directionality for the reference sample. In contrast, if the $\mathrm{PVA_{R6G}}$–Ag sample is excited with $\theta_{\mathrm{exc}} = 5^{\mathrm{o}}$ (Fig. 2d), the presence of Ag substrates greatly alters the appearance of the fluorescence directionality, where a pronounced forward beaming effect is observed for the s-polarized emission, while the p-polarized fluorescence intensity immediately declines after $\theta_{\mathrm{FL}} = 30^{\mathrm{o}}$. If excited with $\theta_{\mathrm{exc}} = 30^{\mathrm{o}}$ (Fig. 2e), the s-polarized emission essentially returns back to the Lambertian appearance, in contrast, the p-polarized emission displays the forward beaming effect. With an even larger excitation angle $\theta_{\mathrm{exc}} = 60^{\mathrm{o}}$ (Fig. 2f), the p-polarized emission of the $\mathrm{PVA_{R6G}}$–Ag sample remains the same as in $\theta_{\mathrm{exc}} = 30^{\mathrm{o}}$. However, the s-polarized fluorescence pattern significantly differs from previous

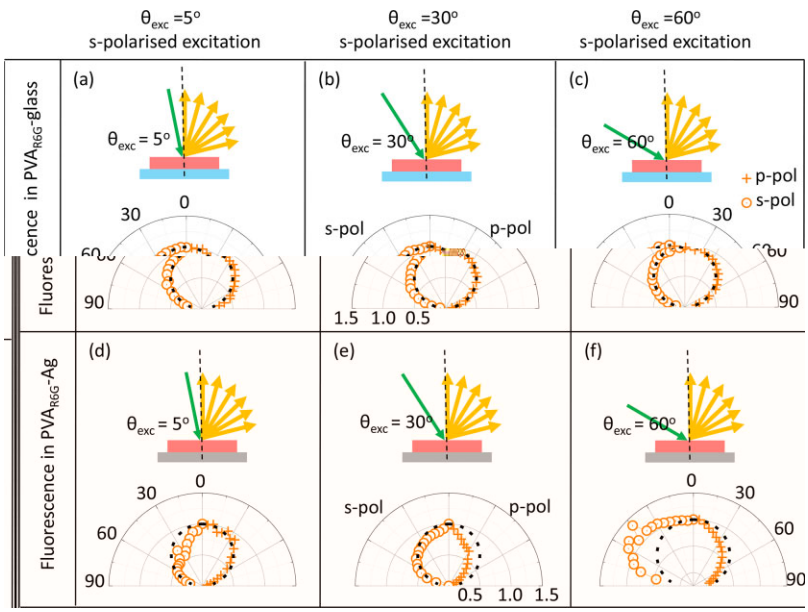

Figure 2 Angular distribution of measured fluorescence intensity for the $\mathrm{PVA_{R6G}}$–glass (upper line) and the $\mathrm{PVA_{R6G}}$–Ag (lower line) sample. The fluorescence intensity at each emission angle is normalized to the intensity at normal emission ($\theta_{\mathrm{FL}} = 0^{\mathrm{o}}$) in each plot. The first column polar plots in (a) and (d) correspond to the fluorescence under s-polarized excitation ($\lambda_{\mathrm{exc}} = 532$ nm) at excitation angle $\theta_{\mathrm{exc}} = 5^{\mathrm{o}}$, the second column (b) and (e) corresponds to the excitation angle $\theta_{\mathrm{exc}} = 30^{\mathrm{o}}$, and the third column (c) and (f) to $\theta_{\mathrm{exc}} = 60^{\mathrm{o}}$. As indicated in the middle polar plots (b) and (e), the left quadrant of each plot corresponds to the s-polarized fluorescence, while the right quadrant to the p-polarized fluorescence. Black dashed lines in each polar plot indicate the calculated Lambertian emission.

cases, exhibiting a very directional radiation towards $\theta_{FL} = 55^{o}$. Obviously, the fluorescence directionality for the PVA_{R6G}–Ag sample displays an unusual dependence on the excitation angles, indicating that the presence of Ag substrates makes emission from the PVA_{R6G}–Ag sample very sensitive to the change of excitation conditions. The direct comparison between emission directionalities under different excitation angles can be found in Fig. S2 in Supporting Information; we also note that the fluorescence directionality can be modified by altering the polarization of the excitation laser; please see Fig. S3 in Supporting Information for details.

Biased emission with respect to the direction of excitation light has been reported in Ag island films embedded with fluorophores [44] possibly due to the strongly orientational scattering ability of the Ag nanoislands. However, in our case, the excitation angle dependent fluorescence directionality is shown in a thin-film cavity without any orientational scatterers. Therefore, it is necessary to find out the factor causing the modification of emission directionality in our structure. As mentioned above and demonstrated in Fig. 1, at $\lambda = 532$ nm, the PVA_{R6G}–Ag sample absorbs more incident energy for higher oblique s-polarized illumination, as a result of the coupling between FP resonances and molecular absorption. Another significance of this coupling is that the spatial distribution of incident energy inside the cavity fluctuates for different illumination angles. The intensity distributions ($|E|^2$) across the thickness (y-axis) of the PVA_{R6G}–Ag sample under s-polarized illumination ($\lambda = 532$ nm) with $\theta_{in} = 5^{o}$ and $\theta_{in} = 60^{o}$ were calculated using the transfer matrix method [45] and are shown in Fig. 3a and b, respectively. In the case of 5^{o} illumination (Fig. 3a), the intensity peaks at $h = 60$ nm (h denotes the fluorophore-interface distance as illustrated in Fig. 3a), whereas under 60^{o} illumination (Fig. 3b), the intensity maximum moves to a higher position, i.e., $h = 90$ nm above the Ag surface. In the process of excitation, the magnitude of incident intensity at a specific h undoubtedly affects the degree of excitation to a molecule at this position. As the result, if the PVA_{R6G}–Ag sample is illuminated at an angle, the molecules in the middle of the PVA_{R6G} coating are most strongly excited, while in the case of, the most strongly excited molecules appears in the position close to the Air-PVA interface. Hence, altering the excitation angle allows us to dynamically tune the excitation efficiency for molecules at different locations.

On the other hand, the overall fluorescence of the PVA_{R6G}–Ag sample is the sum of emission from dye molecules at all locations. Previous studies [27, 31, 32, 35, 46, 47] and our Finite-Difference Time-Domain (FDTD)

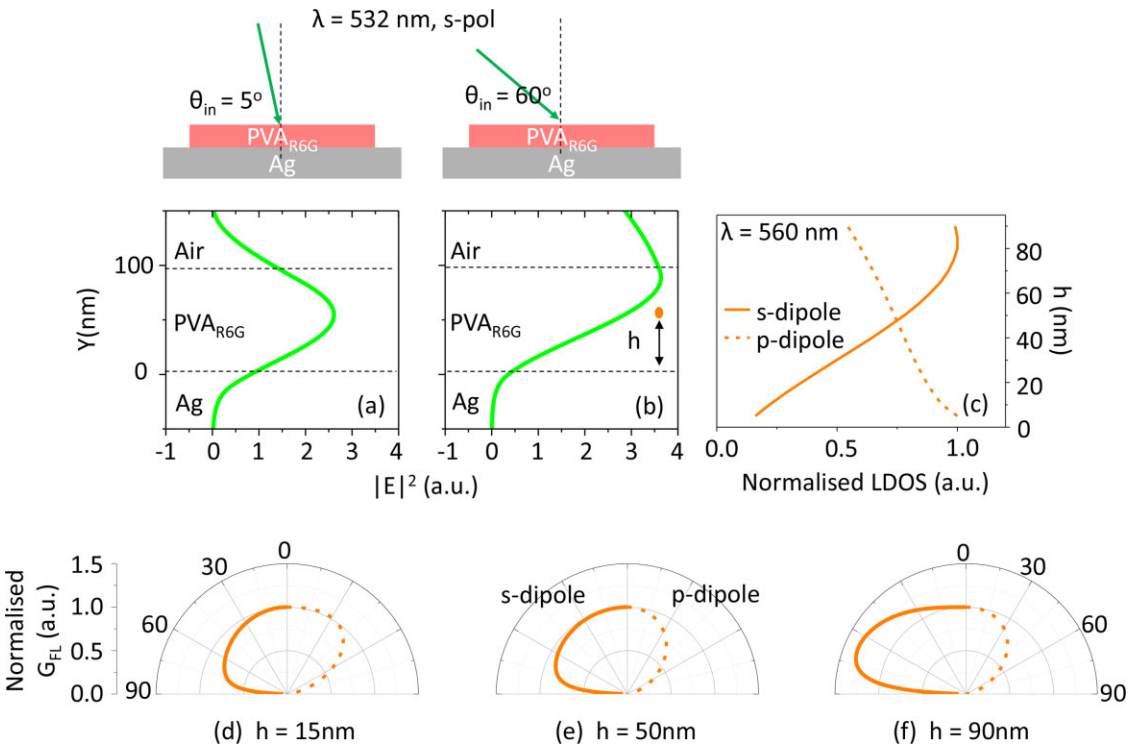

Figure 3 Insights for different illumination angles: the variation of excitation waves and optical properties of dye molecules at different locations. (a,b) Simulated intensity distribution across the thickness of the PVAR6G–Ag sample illuminated by s-polarized light with incident angle $\theta_{in} = 5^{o}$ (a) and $\theta_{in} = 60^{o}$ (b) at the excitation wavelength $\lambda = 532$ nm. (c) LDOS as a function of h for s- and p-dipole at the wavelength $\lambda = 560$ nm. (Please see text for details.) (d–f) Calculated radiation directionality of a dipole at the position $h = 15$nm (d), $h = 50$ nm (e), and $h = 90$ nm (f) for s- (left quadrant) and p- (right quadrant) polarized dipole at the wavelength $\lambda = 560$ nm. [h is defined as the dipole–Ag substrate distance as illustrated in Fig. S4.]

simulations (Fig. S5 in Supporting Information) reveal that the emission properties of dye molecules are significantly dependent on the positions (h) and the orientations of molecules. Specifically, due to the coupling between excited fluorophores in the PVA_{R6G}–Ag sample and the FP resonances in the cavity, the SPPs propagating along the PVA_{R6G}–Ag interface and the intrinsic absorption of Ag substrates, the Local Density of Optical States (LDOS) inside the structure varies with dipole locations and orientations. Figure 3c shows the normalized LDOS for s- and p- dipole as a function of h simulated by the FDTD method. The orientation of molecules is usually assumed to be isotropic. For simplicity, here we denote the dipole contributing to s-polarized emission as s-dipole, which has the orientation perpendicular to the plane of incidence, and denote the one causing p-polarized emission as p-dipole, which includes all orientations in parallel with the plane of incidence, (for details of the molecular orientation and the calculation of LDOS, please see Fig. S4 and the section "Modelling of LDOS" in the Supporting Information). In particular, the normalized LDOS for s-dipole increases towards larger values of h until $h = 85$ nm, whereas for p-dipole the LDOS declines monotonically with the increasing h value. As a result, photons emitted by fluorophores at different locations contribute to the overall fluorescence with various degrees, since it is well known that the spontaneous emission rate of an excited fluorophore is proportional to the LDOS [48].

In addition, dye molecules at different position h exhibit various radiation directionalities, because the interference behavior between the fluorophore radiation and the reflected waves from the reflecting surface also significantly depends on h as well as the dipole orientation of molecules [35]. We then simulated the radiation directionalities for s- and p- dipole in the spectral position ($\lambda = 560$ nm) at $h = 15$ nm, $h = 50$ nm, and $h = 90$ nm in the PVA_{R6G}–Ag structure, as shown in Fig. 3d–f, respectively. The simulations were performed by calculating the normalized fluorescence enhancement $G(\theta_{FL})$ as a function of emission angle, for dipoles at different positions h, using the principle of reciprocity as proposed in Refs. [20, 29]. Specifically, the radiation of s-dipoles, corresponding to s-polarized emission, exhibits a significant directional enhancement towards $\theta_{FL} = 60^{o}$ as the dipole-interface distance h increases. In contrast, the p-dipoles, contributing to p-polarized emission, at $h = 15$ nm radiate more to, but this directional radiation disappears when $h = 90$ nm. If we compare Figure 3d, 3e and 3f with Fig. 2d, 2e, and 2f respectively, we can find that the emission directionality for the PVA_{R6G}–Ag sample under different excitation angles shows a similar variation tendency to the dipole radiation at different h positions. We also note that the fluorescence lifetime measured on the PVAR6G–Ag sample varies with collection angle θ_{FL}; please see Fig. S6 in Supporting Information for more details.

As discussed above, the intensity distribution of excitation wave, the LDOS and the radiation from individual dipoles all contribute to the overall fluorescence. We therefore can mathematically express the angular distribution of fluorescence from the PVA_{R6G}–Ag sample under different excitation angles by using Equation (2)

$$I_{\alpha}(\theta_{exc}, \theta_{FL}) = \frac{1}{d}\int_{0}^{d} |E^{\beta}_{exc}(\theta_{exc}, h)|^{2} \times \mathrm{norm}[G_{\alpha}(\theta_{FL}, h)] \cdot \mathrm{LDOS}_{\alpha}(h)\mathrm{d}h, \quad (2)$$

where $G_{\alpha}(\theta_{FL}, h)$ and $\mathrm{LDOS}_{\alpha}(h)$ as functions of h denote the fluorescence enhancement and local density of states with a polarization α, respectively. The influence of the excitation wave $|E^{\beta}_{exc}(\theta_{exc}, h)|^{2}$ as a function of excitation angle θ_{exc} and the position h, with polarization β has been also included. Using Equation (2), we calculated the fluorescence directionality for the PVA_{R6G}–Ag sample excited by s-polarized illumination with, 30^{o} and 60^{o} shown in Fig. 4. Comparing with the experimental results in Fig. 2d–f, we find that the simulated polar patterns show a similar tendency, i.e., as the excitation angle increases, the s-polarized emission displays a directional radiation towards the angle range between $\theta_{FL} = 50^{o}$ and $\theta_{FL} = 65^{o}$, while the p-polarized emission intensity exhibits an unobvious forward beaming effect, with steeper decrease at higher excitation angles. However, we also note that the experimental results (Fig. 2d–f) are more pronounced than the simulated integration results (Fig. 4) and share more similarities with the simulated radiation patterns of dipoles at fixed positions (Fig. 3d–f for $h = 15$, 50, and 90 nm respectively). This is possibly due to the inhomogeneous distribution of dye molecules across the thickness of the PVA_{R6G} coating [49], or the preferential orientation of dye molecules close to the Ag substrate [35]. But the key principle of this newly-discovered phenomenon is well described by the theory and analysis. In addition, this phenomenon also suggests that the directional emission beaming effect can be further enhanced by elaborating the designs of the PVA_{R6G}–Ag cavities, e.g., multilayer architectures that allow stratifying and locating dye molecules at fixed distances above the reflecting surface.

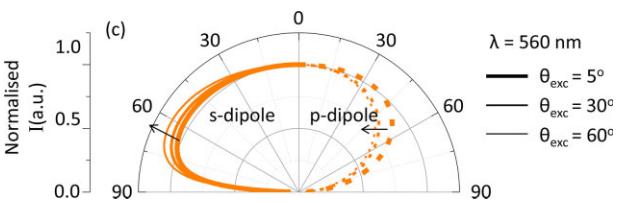

Figure 4 The calculated overall radiation directionality of a PVAR6G-Ag sample at the wavelength $\lambda = 560$ nm, under s-polarized excitation with different excitation angle (θ_{exc}) by integrating dipoles at all positions (h) using Eq. (2).

4 Conclusion In conclusion, we have designed and fabricated a fluorophore-embedded thin-film structure, comprising of a $\sim\lambda/4n$ thick PVA coating doped with R6G molecules on an optically thick Ag substrate, the fluorescence properties of which can be dynamically tuned by altering the excitation conditions. Specifically, the fluorescence intensity is enhanced with respect to a glass substrate reference sample, and the strength of enhancement can be manipulated by adjusting the illumination angle of the excitation laser. Additionally, changing the excitation angles and polarization directionally redistributes the fluorescence intensity from the PVA_{R6G}–Ag sample, with both forward-enhanced (beaming) and forward-suppressed intensity distributions achievable. By comparing the fluorescence spectra with absorption spectra, we find the fluorescence enhancement directly relates to the absorbing efficiency of the PVA_{R6G}–Ag sample, which is very sensitive to the illumination angle, as a result of coupling between the molecular absorption and FP resonances. On the other hand, the intensity distribution of the excitation wave within the PVA_{R6G}–Ag sample fluctuates with different excitation angles. As the result, the excitation efficiency for molecules at different locations can be modified by altering the excitation angle, which gives the rise to the modification of the overall emission directionality.

This fluorophore-embedded thin-film system offers a new conceptual platform for dynamically manipulating fluorescence emission properties. The mechanism of such a cavity can also be applied in electroluminescence systems, e.g., stratified organic light-emitting diodes. In addition, more sophisticated and finer control of emission directionality and enhancement may be achieved by using patterned substrates. Due to the relatively inexpensive and large-area fabrication process, the light emitting thin-film structure opens up broad prospects for many real life applications, e.g., light emitting devices [37] that allow tuneable directional lighting, plasmonic lasers [7, 25] with controllable emission intensity or bio-sensing systems that can highlight the fluorescence readout by tuning the directional emission.

Supporting Information

Additional supporting information may be found in the online version of this article at the publisher's website.

Acknowledgements The authors would like to acknowledge Dr. Nikita Arnold and Prof. Shanhui Fan for discussions and Xing Lin and Prof. Limin Tong for excellent technical support. This work was financially supported by New Zealand's Marsden Fund through contract UOO-1214, the National Natural Science Foundation of China (grants 61275030, 61205030, and 61235007), the Opened Fund of State Key Laboratory of Advanced Optical Communication Systems and Networks, and the Swedish Foundation for Strategic Research (SSF) and the Swedish Research Council (VR).

References

[1] J. A. Schuller, E. S. Barnard, W. Cai, Y. C. Jun, J. S. White, and M. L. Brongersma, Nature Mater. **9**, 193 (2010).
[2] P. P. Pompa, L. Martiradonna, A. Della Torre, F. Della Sala, L. Manna, M. De Vittorio, F. Calabi, R. Cingolani, and R. Rinaldi, Nature Nanotechnol. **1**, 126 (2006).
[3] M. Schmelzeisen, Y. Zhao, M. Klapper, K. Müllen, and M. Kreiter, ACS Nano **4**, 3309 (2010).
[4] A. Kinkhabwala, Z. Yu, S. Fan, Y. Avlasevich, K. Müllen, and W. E. Moerner, Nature Photon. **3**, 654 (2009).
[5] M. A. Noginov, G. Zhu, A. M. Belgrave, R. Bakker, V. M. Shalaev, E. E. Narimanov, S. Stout, E. Herz, T. Suteewong, and U. Wiesner, Nature **460**, 1110 (2009).
[6] N. Arnold, B. Ding, C. Hrelescu, and T. A. Klar, Beilstein J. Nanotechnol. **4**, 974 (2013).
[7] T. Zhai, X. Zhang, Z. Pang, X. Su, H. Liu, S. Feng, and L. Wang, Nano Lett. **11**, 4295 (2011).
[8] H. Gersen, M. F. García-Parajó, L. Novotny, J. A. Veerman, L. Kuipers, and N. F. van Hulst, Phys. Rev. Lett. **85**, 5312 (2000).
[9] D. Vercruysse, X. Zheng, Y. Sonnefraud, N. Verellen, G. Di Martino, L. Lagae, G. A. E. Vandenbosch, V. V Moshchalkov, S. A. Maier, and P. Van Dorpe, ACS Nano **8**, 8232 (2014).
[10] T. H. Taminiau, F. D. Stefani, F. B. Segerink, and N. F. van Hulst, Nature Photon. **2**, 234 (2008).
[11] H. J. Lezec, A. Degiron, E. Devaux, R. A. Linke, L. Martin-Moreno, F. J. Garcia-Vidal, and T. W. Ebbesen, Science **297**, 820 (2002).
[12] A. G. Curto, G. Volpe, T. H. Taminiau, M. P. Kreuzer, R. Quidant, and N. F. van Hulst, Science **329**, 930 (2010).
[13] H. Aouani, O. Mahboub, N. Bonod, E. Devaux, E. Popov, H. Rigneault, T. W. Ebbesen, and J. Wenger, Nano Lett. **11**, 637 (2011).
[14] H. Aouani, O. Mahboub, E. Devaux, H. Rigneault, T. W. Ebbesen, and J. Wenger, Nano Lett. **11**, 2400 (2011).
[15] N. Y. Yu, J. F. Fan, Q. J. Wang, C. Pflügl, L. Diehl, T. Edamura, Y. Masamichi, H. Kan, and F. Capasso, Nature Photon. **2**, 564 (2008).
[16] G. Vecchi, V. Giannini, and J. Gómez Rivas, Phys. Rev. Lett. **102**, 146807 (2009).
[17] B. Ding, C. Hrelescu, N. Arnold, G. Isic, and T. A. Klar, Nano Lett. **13**, 378 (2013).
[18] J. Y. Suh, C. H. Kim, W. Zhou, M. D. Huntington, D. T. Co, M. R. Wasielewski, and T. W. Odom, Nano Lett. **12**, 5769 (2012).
[19] W. Zhou, M. Dridi, J. Y. Suh, C. H. Kim, D. T. Co, M. R. Wasielewski, G. C. Schatz, and T. W. Odom, Nature Nanotechnol. **8**, 506 (2013).
[20] E. Almpanis, N. Papanikolaou, G. Gantzounis, and N. Stefanou, J. Opt. Soc. Am. B **29**, 2567–2574(2012).
[21] J. R. Lawrence, Y. Ying, P. Jiang, and S. H. Foulger, Adv. Mater. **18**, 300–303 (2006).
[22] H. Ding, Y. Cheng, H. Gu, Y. Zhao, B. Wang, and Z. Gu, Nanoscale **5**, 11572–11576 (2013).
[23] T. Neal, K. Okamoto, and A. Scherer, Opt. Express **13**, 5522 (2005).
[24] M. C. Gather, K. Meerholz, N. Danz, and K. Leosson, Nature Photon. **4**, 457 (2010).
[25] P. Berini and I. De Leon, Nature Photon. **6**, 16 (2011).

[26] B. Ding, M. Qiu, and R. J. Blaikie, Opt. Express **22**, 25965 (2014).
[27] J. R. Lakowicz, Anal. Biochem. **337**, 171 (2005).
[28] P. Andrew and W. L. Barnes, Science **306**, 1002 (2004).
[29] L. Luan, P. R. Sievert, W. Mu, Z. Hong, and J. B. Ketterson, New J. Phys. **10**, 073012 (2008).
[30] M. Noginov, G. Zhu, M. Mayy, B. Ritzo, N. Noginova, and V. Podolskiy, Phys. Rev. Lett. **101**, 226806 (2008).
[31] W. L. Barnes, J. Mod. Opt. **45**, 661 (1998).
[32] G. Cnossen, K. E. Drabe, and D. A. Wiersma, J. Chem. Phys. **98**, 5276 (1993).
[33] M. Lieberherr, C. Fattinger, and W. Lukosz, Surf. Sci. **189/190**, 954 (1987).
[34] K. H. Drexhage, Surf. Sci. **1**(2), 693 (1970).
[35] Y. Ishibashi, S. Ohshima, and T. Kajiwara, Surf. Sci. **201**, 311 (1988).
[36] Z. Xi, Y. Lu, P. Yao, W. Yu, P. Wang, and H. Ming, Opt. Express **21**, 30327 (2013).
[37] G. M. Akselrod, B. J. Walker, W. A. Tisdale, M. G. Bawendi, and V. Bulovic, ACS Nano **6**, 467 (2012).
[38] N. Danz, J. Heber, A. Bräuer, and R. Kowarschik, Phys. Rev. A **66**, 063809 (2002).
[39] Y. Cesa, C. Blum, J. M. van den Broek, A. P. Mosk, W. L. Vos, and V. Subramaniam, Phys. Chem. Chem. Phys. **11**, 2525 (2009).
[40] C. Blum, N. Zijlstra, A. Lagendijk, M. Wubs, A. P. Mosk, V. Subramaniam, and W. L. Vos, Phys. Rev. Lett. **109**, 203601 (2012).
[41] R. R. Chance, J. Chem. Phys. **60**, 2744 (1974).
[42] M. Kreiter, M. Prummer, B. Hecht, and U. P. Wild, J. Chem. Phys. **117**, 20 (2002).
[43] K. G. Lee, X. W. Chen, H. Eghlidi, P. Kukura, R. Lettow, A. Renn, V. Sandoghdar, and S. Gotzinger, Nature Photon. **5**, 166 (2011).
[44] K. Aslan, S. N. Malyn, and C. D. Geddes, Chem. Phys. Lett. **453**, 222 (2008).
[45] I. J. Hodgkinson and Q. Wu, Birefringent Thin Films and Polarizing Elements (World Scientific, Singapore, 1997).
[46] N. Calander, J. Phys. Chem. B **109** 13957, (2005).
[47] I. Gryczynski, J. Malicka, K. Nowaczyk, Z. Gryczynski, and J. R. Lakowicz, J. Phys. Chem. B **108** 12073, (2004).
[48] B. Novotny and L. Hecht, Principles of Nano-Optics (Cambridge University Press, Cambridge. 2012).
[49] H. Wang, A. M. Bardo, M. M. Collinson, and D. A. Higgins, J. Phys. Chem. B **102**, 7231 (1998).